On the application of SPH to solid mechanics

IOP Conf. Series: Journal of Physics: Conf. Series **1268** (2019) 012077 doi:10.1088/1742-6596/1268/1/012077

On the application of SPH to solid mechanics

Alexey Shutov[1,2] **and Vladislav Klyuchantsev**[1,2]

[1] Lavrentyev Institute of Hydrodynamics, pr. Lavrentyeva 15, 630090, Novosibirsk, Russia
[2] Novosibirsk State University, ul. Pirogova 1, 630090, Novosibirsk, Russia

E-mail: alexey.v.shutov@gmail.com

Abstract. We analyze the applicability of the smooth particle hydrodynamics (SPH) to the solution of boundary value problems involving large deformation of solids. The main focus is set on such issues as the reduction of artificial edge effects by implementing corrected kernels and their gradients, accurate and efficient computation of the deformation gradient tensor, evaluation of the internal forces from the given stress field. For demonstration purposes, a hyperelastic body of neo-Hookean type and a visco-elastic body of Maxwell type are considered; the formulation of the Maxwell material is based on the approach of Simo and Miehe (1992). For the implementation of constitutive relations efficient and robust numerical schemes are used. A solution for a series of test problems is presented. The performance of the implemented algorithms is assessed by checking the preservation of the total energy of the system. As a result, a functional combination of SPH-techniques is identified, which is suitable for problems involving large strains, rotations and displacements coupled to inelastic material behaviour. The accuracy of the SPH-computations is assessed using nonlinear FEM as a benchmark.

1. Introduction

Smoothed Particle Hydrodynamics (SPH) is a mesh-free discretization method used for boundary value problems of continuum mechanics. In the last decades there has been a large progress in the SPH-simulation of solid dynamics, including both elasticity and inelasticity [6, 9]. The advantages of SPH over the conventional FEM is that SPH procedures are more robust with respect to large distorsions of the body. This make the SPH especially attractive in problems of fracture mechanics and mechanics of multi-phase media. In case of solids, there is a certain similarity between SPH and peridynamics [3]. The drawbacks of SPH are the low accuracy of approximation of discontinuous functions, edge effects, need to suppress non-physical instabilities by introducing an artificial viscosity. Another disadvantage of SPH lies in a low order of convergence for derived fields like strains and stresses [8]. In [2], various corrected smoothing kernels and corrected kernel gradients are considered to increase the order of approximation of derived variables. Moreover, a simplified computationally efficient correction of the kernel is suggested in [2]. Since the simplified correction of the kernel is incomplete, the authors use an additional correction of the kernel gradients. As a byproduct, such a correction allows one to reduce the undesired edge effect. In contrast to [2] and [8], we use a full correction of the smoothing kernel in a combination with a straightforward gradient of the corrected kernel. This aspect defines the novelty of the current work. The well-known $\{\mathbf{F}, \mathbf{p}\}$-approach is implemented here (cf. [8]), whereas the primary discretization quantities are the deformation gradient and the linear momentum. Two different approaches to the computation of the deformation gradient $\mathbf{F}$ can be used. The first one yields the deformation gradient as a straightforward derivative of the

displacement with respect to the referential position vector (see (8)) and the second one is based on the integration of a corresponding evolution equation (see (9)). The choice between different alternatives depends on the application. The first approach is free from accumulation of the integration error but the second one is suitable for problems with contact (self-contact). Apart from different methods for $\mathbf{F}$, the SPH-literature contains a big number of ways to compute the vector of internal forces and to stabilize the computations. The goal of the current contribution is to report a suitable combination of various modelling techniques and to demonstrate its applicability to problems of solid mechanics.

2. Smoothing kernel

For SPH, it was initially suggested to use the Gaussian kernel [10], but in the follow-up studies the cubic spline [9],[8] was advocated due to a reduced computational effort. In this paper, the following kernel will be taken:

$$W(h,q) = \frac{10}{7\pi h^2}\begin{cases} 1-\frac{3}{2}q^2+\frac{3}{4}q^3, & \text{if } 0\le q\le 1,\\ \frac{1}{4}(2-q)^3, & \text{if } 1\le q\le 2,\\ 0, & \text{otherwise,}\end{cases}$$

where $q = \dfrac{\|\mathbf{x}_a-\mathbf{x}_b\|}{h}$ and $h = \mathrm{k}\cdot\left(\frac{m}{\rho}\right)^{\frac{1}{d}}$. Here, k is a non-dimensional numerical parameter $\mathrm{k}\in[1;1.4]$, d is the dimension of the problem ($d=2$ for the plane strain considered here).

2.1. Kernel correction

Liu proposed a modified kernel [2] to ensure that polynomial functions interpolate accurately to a given degree. The corrected kernel $\widetilde{W}_b(\mathbf{x})$ takes the form:

$$\widetilde{W}_b(\mathbf{x}) = W_b(x)\alpha(\mathbf{x})[1+\boldsymbol{\beta}(\mathbf{x})\cdot(\mathbf{x}-\mathbf{x}_b)], \tag{1}$$

$$\boldsymbol{\beta}(\mathbf{x}) = \Big[\sum_b V_b(\mathbf{x}-\mathbf{x}_b)\otimes(\mathbf{x}-\mathbf{x}_b)W_b(\mathbf{x})\Big]^{-1}\sum_b V_b(\mathbf{x}_b-\mathbf{x})W_b(\mathbf{x}), \tag{2}$$

$$\alpha(\mathbf{x}) = \frac{1}{\sum_b V_b[1+\boldsymbol{\beta}(\mathbf{x})\cdot(\mathbf{x}-\mathbf{x}_b)]W_b(\mathbf{x})}. \tag{3}$$

The gradient of the corrected kernel $\nabla\widetilde{W}_a(x_b)$ can be approximated by the finite difference

$$(\nabla\widetilde{W}_a(\mathbf{x}_b))_\beta \approx \frac{\widetilde{W}(\mathbf{x}_a+dh\ \mathbf{e}_\beta-\mathbf{x}_b)-\widetilde{W}(\mathbf{x}_a-\mathbf{x}_b)}{dh},\quad \beta=\overline{1,2},\quad \mathbf{e}_1=(1,0),\quad \mathbf{e}_2=(0,1), \tag{4}$$

where dh is a small real number; $a,b=\overline{1,N}$; N is the number of particles approximating the body.

3. Smoothed Particle Hydrodynamics (SPH) approximation

Following [2], the vector of internal forces $\mathbf{T}$ will be:

$$\mathbf{T}_a = -\sum_b V_b\ \boldsymbol{\sigma}_b\ \nabla\widetilde{W}_{ba}, \tag{5}$$

where a and b are the particle numbers, $\boldsymbol{\sigma}_b$ is the Cauchy (true) stress at the particle b, $\widetilde{W}_{ba}=\widetilde{W}_b(\mathbf{x}_a)$, $\nabla\widetilde{W}_{ba}=\nabla\widetilde{W}_b(\mathbf{x}_a)\neq\nabla\widetilde{W}_{ab}$, V_b is the volume corresponding to particle b.

Note that there are alternative expressions for the internal force $\mathbf{T}_a$, cf. equation (59) in [2] and equation (30) in [8].

The velocity gradient at particle a is computed through

$$\mathbf{L}_a = \sum_b V_b \ \mathbf{v}_b \otimes \nabla \widetilde{W}_{ab}. \tag{6}$$

Other ways of computing the velocity gradient can be found in the literature as well (see equation (55) in [2]). The kinetic energy K, the potential energy U, and the total energy E are estimated as

$$K = \frac{1}{2} \ \sum_b \rho V_b \mathbf{v}_b \cdot \mathbf{v}_b, \quad U = \sum_b V_b U_b, \quad E = K + U, \tag{7}$$

where ρV_b is the mass of the particle b; U_b is the potential (free) energy per unit volume in the reference configuration at particle b (see (12)).

Two different approaches to the computation of the deformation gradient $\mathbf{F}$ can be used. The referential approach employs relation (see [3])

$$\mathbf{F}_a = \sum_b V_b^{(R)} (\mathbf{u}_b - \mathbf{u}_a) \otimes \nabla \widetilde{W}_{ab}^{(R)} \ + \mathbf{1}, \tag{8}$$

where $\mathbf{u}$ is the displacement vector. Its advantage is low computational cost, since the field $\nabla \widetilde{W}_{ab}^{(R)}$ corresponds to the reference configuration and it is calculated just once. Note that instead of using the displacement vector $\mathbf{u}$ one may compute $\mathbf{F}$ as a function of the current position vector $\mathbf{x}$ (see [8]). Still, we prefer using (8) since it provides more accurate results at $t = 0$. However, this referential approach does not account for the change in the topology like the collision/separation and the self-contact. As an alternative, one may calculate the deformation gradient tensor in the current configuration, integrating the following evolution equation (see, for example, [14])

$$\dot{\mathbf{F}} = \mathbf{L}\mathbf{F}, \quad \Rightarrow \quad \mathbf{F}_a^{n+1} = \exp(\Delta t \ \mathbf{L}_a) \ \mathbf{F}_a^n, \quad \Delta t = t_{n+1} - t_n. \tag{9}$$

4. Material models

4.1. Hyperelastic compressible neo-Hookean material

The Jacobian J, the left Cauchy-Green tensor $\mathbf{B}$, and its unimodular part $\overline{\mathbf{B}}$ are defined through

$$J = \det(\mathbf{F}), \quad \mathbf{B} = \mathbf{F} \ \mathbf{F}^{\mathrm{T}}, \quad \overline{\mathbf{B}} = J^{-\frac{2}{3}} \mathbf{B}. \tag{10}$$

In the neo-Hookean material the deviatoric part of the Kirchhoff stress $\boldsymbol{\tau}$ is proportional to the deviatoric part of $\mathbf{B}$. The volumetric part of $\boldsymbol{\tau}$ is a function of J. Here we use the volumetric part proposed by Hartmann and Neff in [7]

$$\boldsymbol{\tau} = \mu \overline{\mathbf{B}}^{\mathrm{D}} + \frac{k}{10}(J^5 - J^{-5}) \cdot \mathbf{1}, \quad \boldsymbol{\sigma} = \frac{1}{J}\boldsymbol{\tau}. \tag{11}$$

Here, μ and k are the shear and bulk moduli, respectively. The corresponding free (potential) energy per unit volume of the reference configuration is given by

$$\psi = \frac{\mu}{2}(\mathrm{tr}\overline{\mathbf{B}} - 3) + \frac{k}{50}(J^5 + J^{-5} - 2). \tag{12}$$

4.2. Maxwell model

Let us recall the formulation of the Maxwell body suggested by Simo and Miehe in [13]. The model kinematics is based on the multiplicative decomposition of the deformation gradient $\mathbf{F}$ into the elastic part $\mathbf{F}_\mathrm{e}$ and the inelastic part $\mathbf{F}_\mathrm{i}$; the tensor $\mathbf{F}_\mathrm{i}$ gives rise to the inelastic Cauchy-Green tensor $\mathbf{C}_\mathrm{i}$:

$$\mathbf{F} = \mathbf{F}_\mathrm{e}\ \mathbf{F}_\mathrm{i}, \quad \mathbf{C}_\mathrm{i} = \mathbf{F}_\mathrm{i}^\mathrm{T}\ \mathbf{F}_\mathrm{i}. \tag{13}$$

The tensor $\mathbf{C}_\mathrm{i}$ is used to capture the state of the material. Using the same hyperelastic potentials as above, the second Piola-Kirchhoff stress $\tilde{\mathbf{T}}$ is computed by

$$\tilde{\mathbf{T}} = \mu\mathbf{C}^{-1}(\overline{\mathbf{C}}\mathbf{C}_\mathrm{i}^{-1})^\mathrm{D} + \frac{k}{10}(J^5 - J^{-5})\mathbf{C}^{-1}, \quad \overline{\mathbf{C}} = J^{-\frac{2}{3}}\ \mathbf{C}. \tag{14}$$

The evolution of the inelastic strain is governed by the ordinary differential equation

$$\dot{\mathbf{C}}_\mathrm{i} = \frac{1}{\eta}\big(\mathbf{C}\tilde{\mathbf{T}}\big)^\mathrm{D}\mathbf{C}_\mathrm{i} = \frac{\mu}{\eta}(\overline{\mathbf{C}}\mathbf{C}_\mathrm{i}^{-1})^\mathrm{D}\mathbf{C}_\mathrm{i}, \tag{15}$$

where η is a material parameter (Newtonian viscosity). An efficient iteration-free update formula was suggested for this evolution equation in [11]. It reads

$${}^{n+1}\mathbf{C}_\mathrm{i} = \overline{{}^{n}\mathbf{C}_\mathrm{i} + \frac{\Delta t\mu}{\eta}\ {}^{n+1}\overline{\mathbf{C}}}. \tag{16}$$

A more general time-stepping formula was proposed for the Maxwell model with the Mooney-Rivlin potential in [12]. Finally, the true stress $\boldsymbol{\sigma}$ is computed as

$$\boldsymbol{\sigma} = \frac{1}{J}\ \mathbf{F}\ \tilde{\mathbf{T}}\ \mathbf{F}^T. \tag{17}$$

5. Global time stepping method

The evolution of the system is governed by the balance of linear momentum in the form

$$\frac{d}{dt}\begin{bmatrix} \dot{\mathbf{x}}_a \\ \mathbf{x}_a \end{bmatrix} = \begin{bmatrix} \mathbf{T}_a/\rho \\ \dot{\mathbf{x}}_a \end{bmatrix}. \tag{18}$$

To integrate this ordinary differential equation, an explicit third order Runge–Kutta method is used [4]. In order to obtain a stable procedure, the Courant condition must be satisfied. The time step size is thus $\Delta t = \mathrm{CFL} \cdot \frac{h}{\max(c_p, \mathbf{v})}$ [5], where $c_p = \sqrt{\frac{k+4/3\cdot\mu}{\rho}}$ is the compressional wave propagation velocity, CFL is the so-called Courant–Friedrichs–Lewy number. In this paper we use $\mathrm{CFL} \approx 0.1 \div 0.4$ to ensure stability.

6. Numerical examples

6.1. Hyperelastic material

As a benchmark problem we simulate the deformation of a square plate under plane strain condition. The in-plane dimensions are 1mm x 1mm. The surface of the plate is free. First, hyperelastic material behaviour is assumed with the following material constants: $\mu = 1.25$ MPa, $k = 5.833$ MPa which corresponds to a compressible material with the Poisson ratio $\nu = 0.4$. The mass density equals $\rho = 3$ t/mm^3. The initial velocity field corresponds to the simple shear (see Figure 1)

$$\mathbf{v}_1 = 0.8\ \mathbf{x}_2\ 1/\mathrm{s}, \quad \mathbf{v}_2 = 0\ \mathrm{mm/s}. \tag{19}$$

The overall process time is 1.2 s. To obtain a reference solution, the problem was solved using

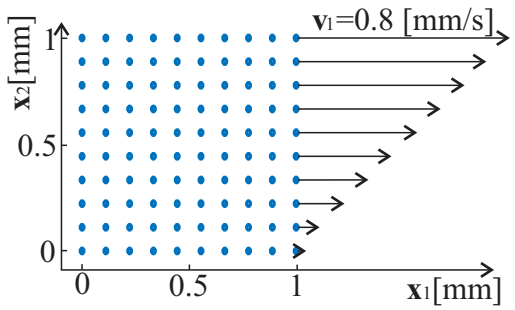

Figure 1. Initial velocity field corresponding to simple shear.

FEM in MSC.MARC. The plate was discretized using a total number of 10x10x1 finite elements with a quadratic approximation of the geometry and displacement. Lamped mass matrix option was activated. The motion equations were integrated using implicit integration procedure with 320 time steps.

To test the current version of the SPH-code, two different discretizations were implemented: with 21x21 and 41x41 equally spaced particles. The obtained displacement of the top-right corner are plotted versus time in Figure 2(left). As can bee seen from the figure, there is a good correspondence between the results provided by FEM and SPH. As expected, the SPH-simulation with a larger number of particles provides displacements closer to the FEM. As mentioned above, the inherent problem of SPH is a low order of approximation of derived quantities like strains and stresses. As is seen from Figure 2(right), the use of corrected smoothing kernels allows one to obtain a reasonable accuracy even when working with large strains, displacements, and rotations. SPH-simulations using 10x10 particles with and without correction of the smoothing kernel were additionally compared to the FEM. The corresponding animation is available under https://youtu.be/O3Ucnv8K6AU .

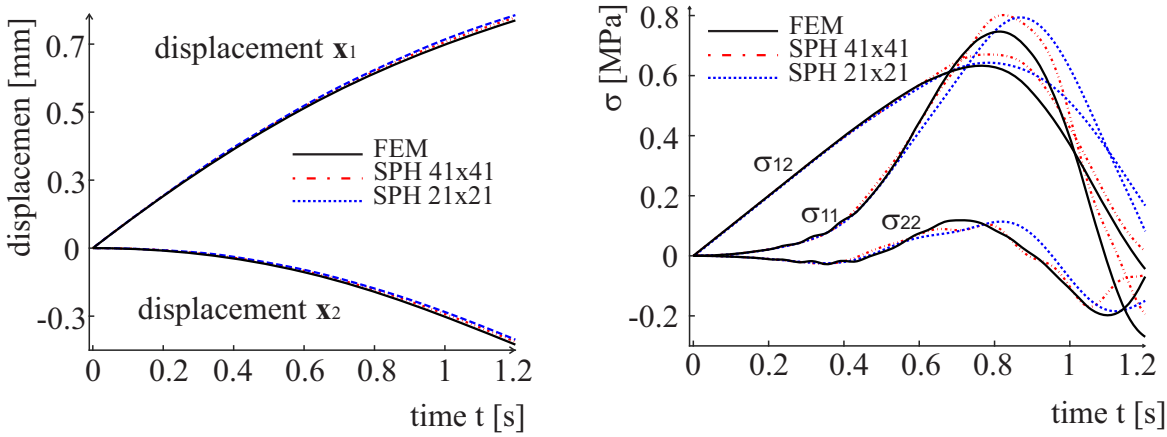

Figure 2. Simulation results on the deformation of a square plate assuming hyperelastic material behaviour obtained by FEM and SPH. Left: displacement of the top-right corner. Right: components of the Cauchy stress in the middle of the plate.

A good means of controlling the plausibility of a computational procedure is to check the preservation of certain integrals (if available). Since the material response is purely hyperelastic, in the current problem, the total energy (7) must remain constant within time. The evolution of the total energy is plotted in Figure 3 for two different SPH-simulations with 11x11 particles.

An impressive result is that the application of the corrected kernel provides a much better preservation of the total energy. At the same time, the SPH with a standard symmetric kernel exhibits nonphysical oscillation of the energy, which can eventually lead to the blow-up of the solution.

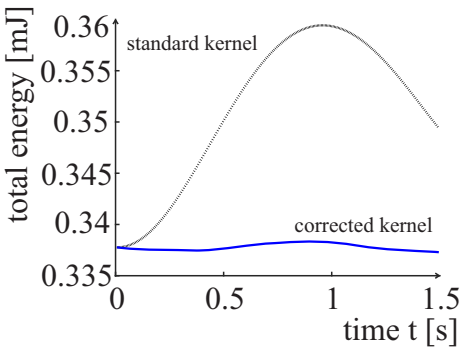

Figure 3. Evolution of the total energy in the SPH-simulation of the deformation of a square plate. Hyperelastic material behaviour is assumed. The use of the corrected kernel allows one to reduce the nonphysical oscillation of the total energy.

6.2. Maxwell material

In this subsection, the applicability of the approach to model an inelastic material behaviour is demonstrated. Toward that end, the Maxwell material from Subsection 4.2 is implemented. The elastic parameters and the mass density are the same as above. Three different values of the Newtonian viscosity are chosen here: $\eta = 1$ MPa $\cdot$ s, $\eta = 1/5$ MPa $\cdot$ s, and $\eta = 1/25$ MPa $\cdot$ s. The deformed geometries of the plate at the final time instance $t = 1.5$ s are shown in Figure 4. For large viscosity η the structure behaves nearly hyperelastic. The structural behaviour represents an oscillation near a rigid body motion (Figure 4, left). For small η the Maxwell material becomes nearly fluid. Thus, the deformation pattern resembles that of the simple shear (Figure 4, right). All the results are consistent with the underlying physics. The animated version of the SPH results is available under https://youtu.be/BeMXNpdqLBY .

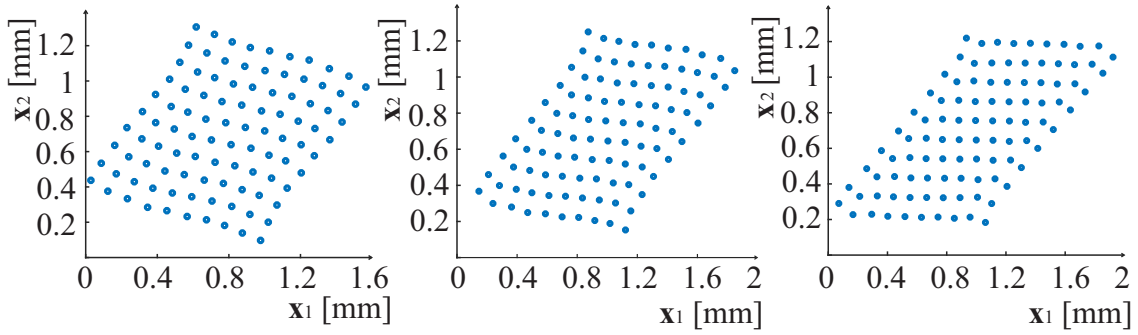

Figure 4. Simulation results for the Maxwell material. Deformed configurations correspond to the final time instance $t = 1.5$ s for different viscosities. Left: $\eta = 1$ MPa $\cdot$ s. Middle: $\eta = 1/5$ MPa $\cdot$ s. Right: $\eta = 1/25$ MPa $\cdot$ s.

7. Conclusion

SPH is considered as a method of spatial discretization for the analysis of solids subjected to large strains, displacements, and rotations. The method is highly promising for nonlinear problems

involving complex rheology, multi-phase media, and non-local material modelling, including plasticity with damage [1]. At the moment, different research groups implement various versions of SPH which essentially differ in the way how they compute the deformation gradient tensor $\mathbf{F}_a$, the vector of interval forces $\mathbf{T}_a$, smoothing kernels, and damping. In the current paper, a fully functional combination of various SPH techniques is tested in terms of hyperelastic and inelastic material models. Corrected smoothing kernels (cf. (1)) with a direct computation of their gradients (cf. (4)) are implemented to reduce the undesired edge effects. Even for a small number of particles, the current version of SPH provides accuracy which is sufficient for engineering applications. One has to bear in mind that the displacements are still computed more accurately than strains and stresses (see Figure 2). The used combination of SPH techniques allows us to consider advanced nonlinear material models going beyond elasticity. The kinematics of the implemented Maxwell body allows for large elastic and inelastic strains. The simulation results do not show any nonphysical behaviour (see Figure 4): The computations are free from nonphysical cohesion of particles as well as tensile and hourglass instabilities frequently observed in such problems (see the discussion in [8]). This is a remarkable result since no damping and artificial viscosities were introduced. Dealing with hyperelastic material response, the current version of SPH preserves the full energy. A generalization of the method to viscoplasticity is straightforward. In conclusion, the SPH with corrected kernels is a versatile tool of numerical analysis allowing for a solution of complex nonlinear problems of solid mechanics.

Acknowledgments

The research was supported by the Russian Science Foundation, project number 19-19-00126.

References

[1] Bažant Z P and Jirásek M 2002 Nonlocal integral formulations of plasticity and damage: survey of progress *J. Eng. Mech.* **128** 1119–49
[2] Bonet J and Lok T-S L 1999 Variational and momentum preservation aspects of smooth particle hydrodynamic formulations *Comput. Methods Appl. Mech. Engrg.* **180** 97–115
[3] Ganzenmuller G C, Hiermaier S and May M 2014 On the similarity of meshless discretizations of peridynamics and smooth-particle hydrodynamics *Comp. Struct.* **170** 71–8
[4] Gottlieb S and Chi-Wang S 1998 Total variation diminishing Runge–Kutta schemes *Math. Comput.* **221** 73–85
[5] Courant R, Friedrichs K and Lewy H 1928 On the partial difference equations of mathematical physics *Math. Ann.* **100** 32–74
[6] Gray J P, Monaghan J J and Swift R P 2001 SPH elastic dynamics *Comput. Methods. Appl. Mech. Egneg* **190** 6641–62
[7] Hartmann S and Neff P 2003 Polyconvexity of generalized polynomial-type hyperelastic strain energy functions for near-incompressibility *Int. J. Solids Struct.* **40** 2767–91
[8] Lee C H, Gil A J, Greto G, Kulasegaram S and Bonet J 2016 A new Jameson–Schmidt–Turkel smooth particle hydrodynamics algorithm for large strain explicit fast dynamics *Comput. Methods Appl. Mech. Engrg.* **311** 71–111
[9] Liu M B and Liu G R 2010 Smoothed particle hydrodynamics (SPH): an overview and recent developments *Arch. Comput. Methods. Eng.* **17** 25–76
[10] Monaghan J J 1992 Smoothed particle hydrodynamics *Annu. Rev. Astron. Astrophys.* **30** 543–74
[11] Shutov A V, Landrgaf R and Ihlemann J 2013 An explicit solution for implicit time stepping in multiplicative finite strain viscoelasticity *Comput. Methods Appl. Mech. Engrg.* **265** 213–25
[12] Shutov A V, 2018 Efficient time stepping for the multiplicative Maxwell fluid including the Mooney–Rivlin hyperelasticity *Int. J. Numer. Meth. Engng.* **113**1851–69
[13] Simo J C and Miehe C 1992 Associative coupled thermoplasticity at finite strains: formulation, numerical analysis and implementation *Comput. Methods Appl. Mech. Engrg.* **98** 41–104
[14] Weber J and Annand L 1990 Finite deformation constitutive equations and a time integration procedure for isotropic, hyperelastic-viscoelastic solids *Comput. Methods Appl. Mech. Engrg.* **79** 173–202